RESEARCH PAPER

Preparation and Characterization of Nanostructured S and Fe co-doped TiO_2 Thin Film by Ultrasonic-assisted Spray Pyrolysis Method

Hossein Rasoulnezhad[1], Ghader Hosseinzadeh[2]*, Javad Yekrang[3]

[1] *Department of Electrical and Electronics Engineering, Standard Research Institute, Karaj, Iran*

[2] *Department of Chemical Engineering, University of Bonab, Bonab, Iran*

[3] *Department of Textile Engineering, University of Bonab, Bonab, Iran.*

ARTICLE INFO

Article History:
Received 03 March 2018
Accepted 11 June 2018
Published 01 July 2018

Keywords:
Co-doped
Spray Pyrolysis
TiO_2
Transparent
Ultrasonic

ABSTRACT

Nanostructured TiO_2 and S and Fe co-doped TiO_2 thin films with high transparency were prepared on glass substrate through ultrasonic-assisted spray pyrolysis technique. The effects of doping on morphological, optical and structural properties of TiO_2 were studied by scanning electron microscopy (SEM), X-ray photoelectron spectroscopy (XPS), X-ray diffraction (XRD), photoluminescence spectroscopy, Raman spectroscopy, and UV-visible absorption spectroscopy techniques. Because of the high uniformity and monodispersity of the prepared thin films, they have high visible light transparency. All of the prepared thin films have anatase crystal structure, however, introduction of the dopants, especially S dopant, in the lattice of TiO_2 creates some structural defects in the TiO_2. Because of the presence of defects as charge trapping center in the structure of the doped TiO_2 samples, these thin films have lower electron–hole recombination rate than undoped TiO_2. Furthermore, simultaneous doping of S and Fe considerably narrows the band gap energy of TiO_2.

How to cite this article
Rasoulnezhad H, Hosseinzadeh G, Yekrang J. Preparation and Characterization of Nanostructured S and Fe co-doped TiO2 Thin Film by Ultrasonic-assisted Spray Pyrolysis Method. J Nanostruct, 2018; 8(3): 251-258. DOI: 10.22052/JNS.2018.03.4

INTRODUCTION

With advantage of having long-term stability, cost-effectiveness, strong catalytic activity, non-toxicity and biocompatibility, TiO_2 has received considerable attention in recent decades [1-3]. This semiconductor is used in various applications like paints, cosmetics, antibacterial and self-cleaning surfaces, water purification, cancer treatment [4]. Recently, most of the researches are focused on improving the optical properties of TiO_2 for renewable energy applications [3]. With a band gap (Eg) ranging from 3.0 to 3.2 eV (i.e., from 413 to 387 nm), TiO_2 has low photosensitivity to visible radiation. Therefore, for efficiently harvesting solar energy by TiO_2, its band gap must be reduced which can be achieved by tailoring its morphology and crystal phase, and by introducing of doping elements [5]. The electron-hole recombination rate is another important factor which has considerable effect on the visible light photoactivity of the TiO_2 and any factor that reduce the electron–hole recombination rate will enhance the photocatalytic activity [6]. To reduce the electron–hole recombination rate and the wide band-gap of TiO_2, a variety of methods such as, incorporation of quantum dots (QDs) [7-9], sensitizing with dyes [10], doping and codoping with metal and non-metal elements [11, 12], and decorating with graphene nanosheets [13], have been extensively studied in recent years. Among them, nonmetal and metal doping has been proved to be an efficient approach [14].

* *Corresponding Author Email: g.hosseinzadeh@bonabu.ac.ir*

Sulfur, unlike other non-metal dopants, can present in more than one oxidation state such as S^{2-}, S^{4+} or S^{6+} in TiO_2, depending on the synthesis conditions and the precursor type [15]. Ti could be replaced with cationic forms of S [16], and O is substituted with anionic S [17]. In sulfur doping, the S atoms can occupy the substitutional and interstitial sites in the TiO_2 lattice and the mixing of S 3p states with valance band of TiO_2 can cause the band gap narrowing [18]. Furthermore, the doping of S element reduces the charge-carrier recombination rate, and increases the number of photo-generated electrons and holes on TiO_2 surface [19]. Another advantage of S doping in TiO_2 is the improvement in thermal stability of anatase phase up to 900 °C [7].

Among various transition metals for TiO_2 doping, Fe seems to be the most appropriate one owing to its unique half-filled electronic configuration, which can reduce the band gap energy through the formation of new intermediate energy levels [20]. Furthermore, ionic radius of Fe^{3+} (0.64 Å) ion is nearly same as that of Ti^{4+} (0.68 Å) and this ion can easily substitute for Ti^{4+} in the crystal structure of TiO_2 [21]. Moreover, Fe^{3+} ions in the TiO_2 lattice can act as traps to capture the photogenerated electrons which result in the reduction of the recombination rate of electron–hole pairs [22].

To avoid the expensive and complex separation of the photocatalyst after degradation proses, TiO_2 in the form of thin film on a substrate are preferred to the TiO_2 nanoparticle suspensions. Semiconductor-based photoactive films are deposited on various substrates of metals, ceramics, silicon wafer, and glass in widespread applications such as solar cells, self-cleaning surfaces, hydrogen production, photocatalysis and air purification [23]. Among these substrates, glass substrate is the most appropriate one because of its excellent chemical stability, high transmittance, and low cost. Transparency is an important requirement in consideration of the potential photocatalytic application of coatings on the buildings and vehicles glass, therefore in recent years, there is considerable interest on the preparation of transparent photoactive films on glass substrate [24, 25].

Over the past decade, many studies have been conducted on the simultaneous doping of TiO_2 with metal and non-metal elements. In this regard, in the present work, S and Fe co-doped TiO_2 thin film with high monodispersity and transparency were deposited on glass substrate through ultrasonic-assisted spray pyrolysis technique, for the first time.

MATERIAL AND METHODS

Materials

The following chemicals were used in this work without further purification: titanium(IV) butoxide (≥97.0% from Sigma-Aldrich), Iron(III) chloride hexahydrate ($FeCl_3 \cdot 6H_2O$, Merck),thiourea (≥99.0% from Sigma-Aldrich), absolute ethanol (99.5% v/v, Merck) and concentrated hydrochloric acid (37 wt %, Merck).

Preparation of the thin films

A schematic diagram of the deposition set-up is shown in Fig. 1. TiO_2 sol solution contaning thiourea (as sulfur source) or Iron(III) chloride was

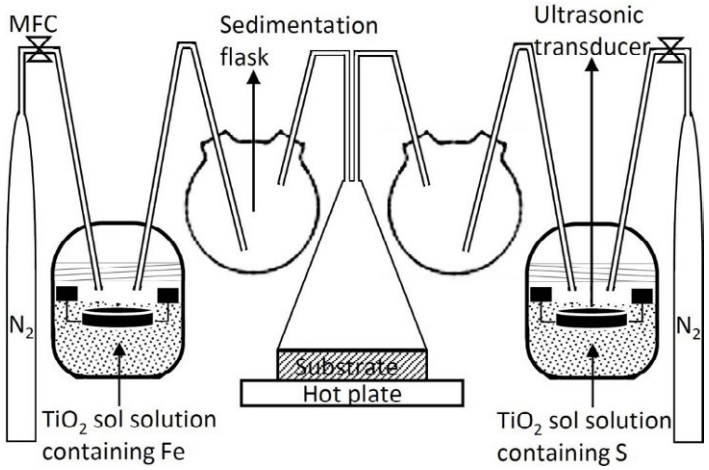

Fig. 1. A schematic view of the ultrasonic-assisted spray pyrolysis technique.

prepared by addition of 40 ml the HCl ethanolic solution (0.01M) into the 30 ml of ethanolic solution of titanium (IV) butoxide (0.71M) in dropwise manner. Amount of thiourea and Iron(III) chloride in TiO_2 sol solution are 61.5 mg, and 171 mg respectively. The pH of the final solutions were adjusted to 2.1 by addition appropriate amount of the HCl ethanolic solution. After about 1 hours stirring, each of the thiourea and iron containing TiO_2 solution were poured into the separate flasks and were sprayed with aid of a floated piezoelectric ultrasonic transducer and were carried by N_2 gas (with flow rate of 300 ml/min). The migrated droplets were thermally decomposed at the surface of the hot glass substrate at 400°C, and the S and Fe co-doped TiO_2 thin film was formed after about 30 min. The presence of sedimentation flask in the deposition set-up is for the improvement of the monodispersity of the thin films by sedimentation of large droplets in its inside.

Characterization

The surface of the prepared thin films were examined using MIRA3 TESCAN field emission scanning electron microscope (FESEM) (Czech Republic). X-ray diffraction (XRD) patterns of the prepared thin films have been recorded by a STOE Stadi diffractometer equipped with Cu-Kα irradiation (λ=1.54018 Å). Photoluminescence (PL) emission spectra of the prepared samples were determined using Cary Eclipse fluorescence spectrophotometer (Varian, Inc., USA) at room temperature, with an excitation wavelength of 300 nm. XPS spectra of the PT0.8 sample were obtained by using a Gammadata-Scienta Esca 200 (Uppsala, Sweden) hemispherical analyzer equipped with an Al Kα (1486.6 eV) X-ray source. All binding energy values were calibrated by using the value of the C 1s peak at 284.6 eV as a reference. Ultraviolet–visible (UV–vis) absorption and transmission spectra of the samples were recorded using Cary 100 Bio spectrophotometer (Varian, Inc., USA). Raman spectra of the samples were obtained using T64000-HORIABA Jobin Yvon Raman spectrometer equipped with an argon ion laser (514 nm).

RESULTS AND DISCUSSION

XRD

The crystalline structure of the undoped and doped TiO_2 thin films were analyzed from the XRD patterns (Fig. 2). In XRD patterns of all samples, the observed diffraction peaks at 2ϑ of about 25.3°, 37.7°, 47.9°, 54.1°, 55.1°, and 62.8°, indexed as (101), (004), (200), (105), (211), and (204) lattice planes, respectively, assigned to the anatase phase of TiO_2 (JCPDS card No. 21-1272). Therfore, all of the prepared thin films have anatase crystalline phase and presence of doped elements don't interfere in the crystal phase of TiO_2. TiO_2 sample shows sharper XRD peaks (indicating a higher crystallinity) than doped TiO_2 thin films. As shown in inset of Fig. 2, compared to the undoped TiO_2 thin film, there is a slight shift to higher diffraction angle and broadening in the (101) XRD peaks of the doped TiO_2 samples which largest shift is observed for the S and Fe co-doped TiO_2 sample. Presence of dopant elements in the lattice of TiO_2 and substitution of Ti or O atoms with these dopants may disrupt the crystalline structure of TiO_2 which results in the defect formation and low crystallization in the doped TiO_2 [26, 27].

Raman spectroscopy

Raman spectroscopy was used as an additional characterization tool to precisely confirm the presence of the trace amounts of the crystal phases of TiO_2 [28]. Room temperature Raman spectra of the prepared samples are shown in Fig. 3. The

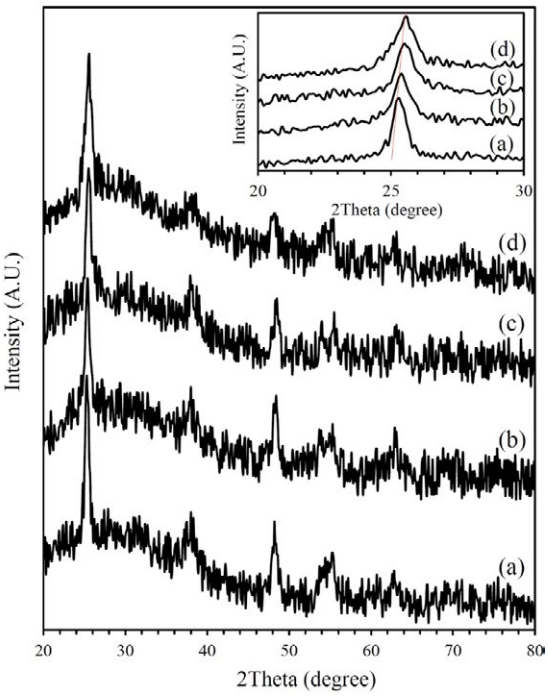

Fig. 2. XRD patterns of (a) TiO_2, (b) Fe doped, (c) S doped and (d) S and Fe co-doped TiO_2 samples.

anatase phase of TiO_2 exhibits five Raman active modes at Eg (144, 197 and 639 cm^{-1}), B1g (395 cm^{-1}), and A1g (513 cm^{-1}) while the rutile phase consists of four Raman-active modes at 143, 233, 447, and 610 cm^{-1} [7, 29]. In the Raman spectra of the pure and doped TiO_2 samples, all of the peaks are assigned to the anatase TiO_2, and there is no peak related to the rutile phase of TiO_2. Hence, the prepared thin films have anatase crystal phase, which are consistent with XRD results. Presence of the oxygen vacancies and formation of defects states can create shift in Raman peaks, as shown in the inset of Fig. 3, there are some shifts in Raman peaks of the S and Fe co-doped and S doped TiO_2 samples, indicating defect formation in these thin films [22, 30, 31].

SEM

Surface morphology of the synthesized thin films was characterized by FESEM and Fig. 4

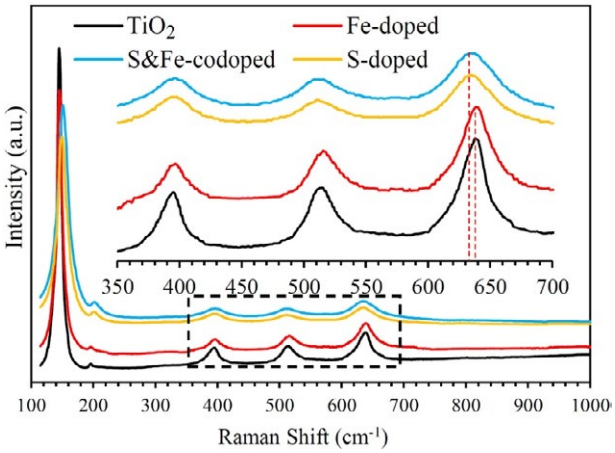

Fig. 3. Raman spectra of the prepared thin films.

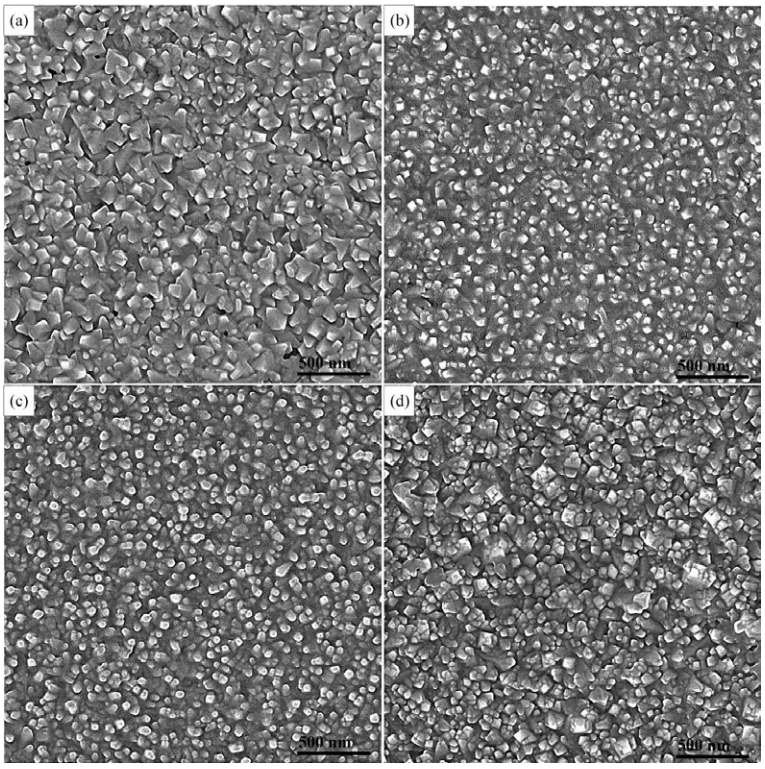

Fig. 4. FE-SEM images of (a) TiO_2, (b) Fe doped, (c) S doped and (d) S and Fe co-doped TiO_2 thin films.

shows FESEM images of the samples at different magnifications. As shown in this figure all of the prepared doped and undoped TiO_2 thin films have nanostructured features, however, compared to the pure TiO_2 thin film, the doped TiO_2 thin films have smaller particles in their structures. Therefore, presence of S and Fe dopants in the TiO_2 lattice hinders further growth of the film particles by disrupting the crystalline structure of TiO_2 as evidenced in XRD and Raman analyzes. Morphologies of the S and Fe co-doped and undoped TiO_2 thin film are irregular shaped nanoparticle, however, some particles with cubic morphology are clearly seen in the structure of S doped and Fe doped TiO_2 thin films. Because of the special design of the deposition set-up, all of the prepared thin films have high monodispersity.

XPS

Fig. 5 depict the S 2p and Fe 2p core-level XPS spectra of the prepared thin films. S 2p core-level XPS spectra of the S and Fe co-doped and S doped TiO_2 samples be deconvoluted into two Gaussian peaks located at the binding energies of about 167.4 and 168.3 eV. According to the literature, the XPS peaks at 167.4 eV depicts the presence of S^{4+} ion in these samples, and the XPS peaks at 168.3 eV the presence of S^{6+} ion in these thin films [7, 18]. Therefore, in these samples, sulfur was doped in the forms of S^{4+} and S^{6+} cations. In Fe 2p core-level XPS spectra of the S and Fe co-doped and Fe doped TiO_2 thin films, there are two peaks at about 712 and 725 eV which belong to the binding energies of Fe $2p_{3/2}$ and Fe $2p_{1/2}$, respectively. The difference of 13 eV between binding energies of Fe $2p_{3/2}$ and Fe $2p_{1/2}$ peaks demonstrates that the oxidation state of Fe in these thin films is +3 [32].

Photoluminescence (PL)

The photocatalytic activity of semiconductor photocatalyst greatly depends on the separation and transfer ability for photoinduced electron–hole pairs. For an irradiated semiconductor sample, the PL intensity is directly related to the electron–hole recombination rate and the high electron–hole recombination rate results in the high PL intensity, and the low photocatalytic performance [33]. Therefore, the efficiency of charge carrier trapping in theprepared samples were investigated by PL spectroscopy. As shown in Fig. 6, all of the doped TiO_2 thin films have lower PL intensity than undoped TiO_2 suggesting an enhanced charge transfer and effective separation of electron-hole pairs in these samples. Among doped samples, the S and Fe co-doped TiO_2 thin film has the lowest PL intensity, therefore

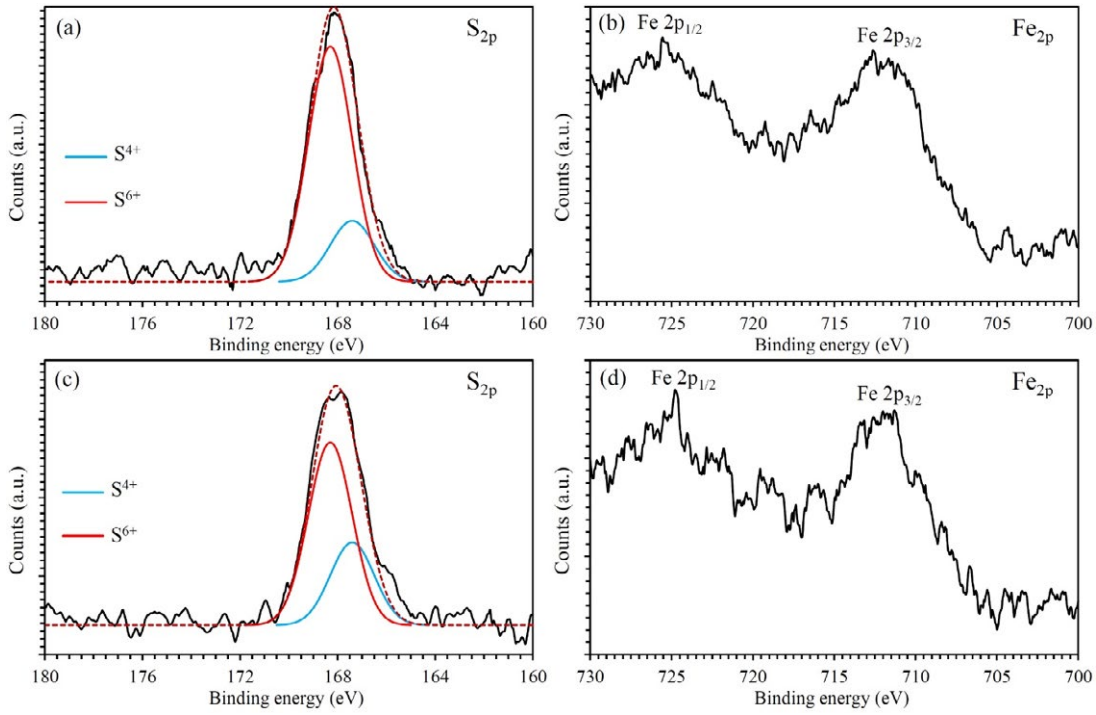

Fig. 5. S 2p and Fe 2p core-level XPS spectra of (a) S-doped, (b) Fe doped, (c) and (d) S and Fe co-doped TiO_2 thin films.

simultaneous presence of S and Fe dopants in the structure of TiO_2 has better effect on charge carriers' separation. Both of oxygen vacancies and lattice defects in the structure of the doped TiO_2 sample can act as charge carrier trapping center and thereby decrease the photoinduced electron–hole recombination rate [34, 35].

Optical properties

Fig. 7(a) depicts the UV–visible absorption spectra of the prepared thin films. Compared with undoped TiO_2, it is obvious that the visible light absorbance intensity of the doped TiO_2 thin films increased. Furthermore, there are noticeable shifts in the absorption edge of the doped TiO_2 samples towards longer wavelengths (red shift), indicating the narrowing of the band gap energy of TiO_2 by doping with S and Fe. The precise value of the band-gap energy (*Eg*) for TiO_2-based semiconductors can be calculated from the intercept of the tangent line to the plots of $(\alpha h\nu)^{1/2}$ versus $h\nu$ (Tauc plots) [36, 37] as shown in Fig. 7(b). The estimated band gap energies of the undoped, S doped, Fe doped, and S and Fe co-doped TiO_2 thin films are 3.16, 2.53, 2.78 and 2.26 eV, respectively. The band gap narrowing of TiO_2 by iron doping can be attributed to (1) a charge transfer transition between TiO_2 valence or conduction band and d electrons of iron or (2) d–d transition in the crystal field depending on the energy levels [30, 38, 39]. According to the previous first-principle calculation studies, introduction of S element to the lattice of TiO_2 induces band gap narrowing by mixing of the S 3p states with the valence band

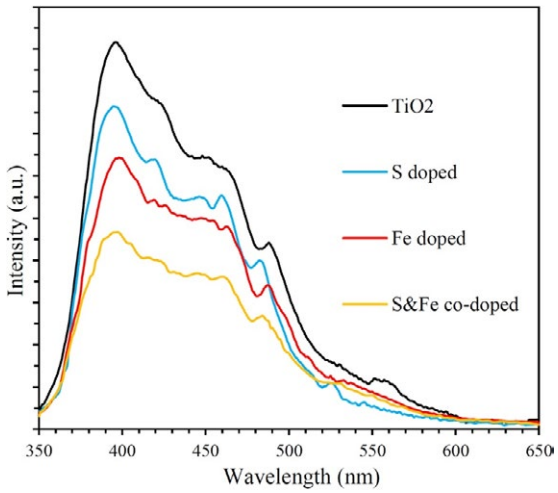

Fig. 6. PL spectra of the prepared TiO_2 thin film samples.

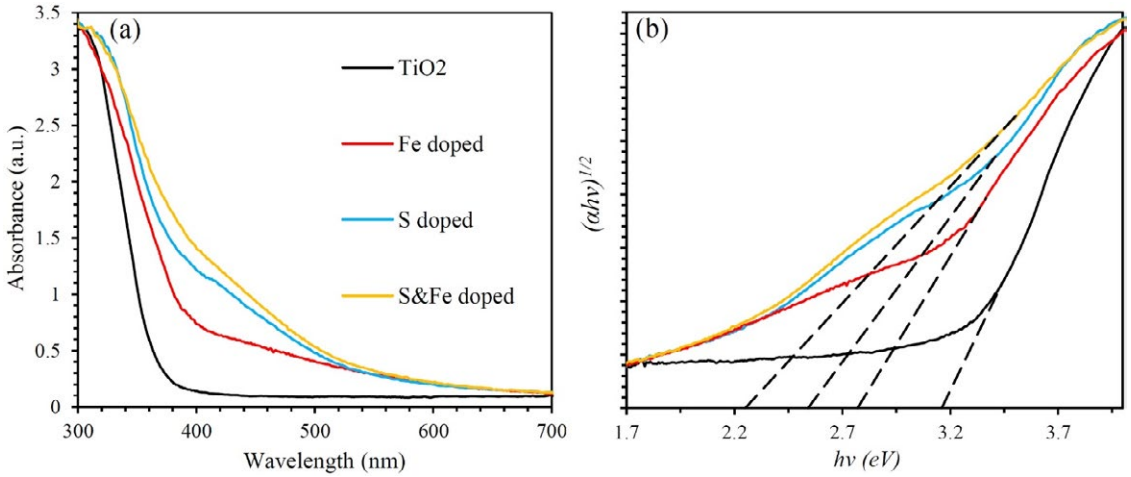

Fig. 7. (a) UV-Vis absorption spectra and (b) band gap energy calculation (Tauc plot) of the prepared thin films.

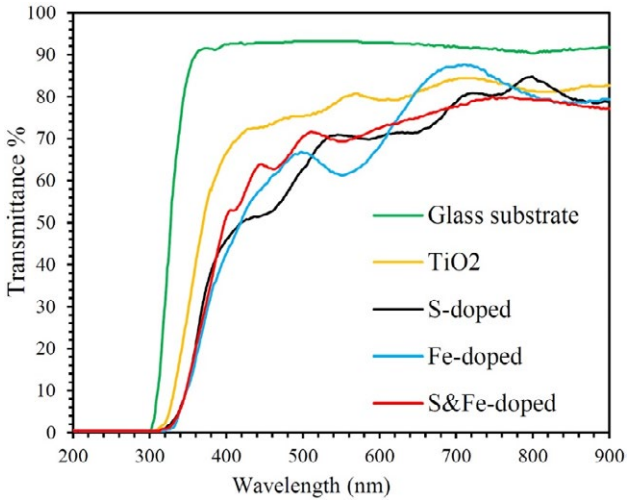

Fig. 8. Transmittance spectra of the prepared thin films.

and localization of S 3p states in the band gap [40, 41]. In the case of S and Fe co-doped TiO_2 thin film, synergic effects of the simultaneous presence of both S and Fe dopants in TiO_2 cause remarkable reduction in the band gap energy of TiO_2.

Transparency of the prepared thin films samples, were examined via UV–Vis transmittance spectroscopy, the results are shown in Fig. 8. As shown in this figure, the transparency of TiO_2, S doped, Fe doped, S and Fe co-doped TiO_2 thin films and glass substrate in visible light region (wavelength of 400-900 nm) are about 79.71 %, 71.62 %, 73.20 %, 71.14 % and 93.40 %, respectively. Therefore, because of the high uniformity and monodispersity of the prepared thin films, they have high transparency in visible light region.

CONCLUSION

In summary, at the present work nanostructured TiO_2 and S and Fe co-doped TiO_2 thin films were deposited on glass substrate through ultrasonic-assisted spray pyrolysis technique. Because of the high uniformity and monodispersity of the prepared thin films, they have high visible light transparency. Both of the undoped and doped TiO_2 have anatase crystal structure, however there are some defect and oxygen vacancies in the doped sample. According to the XPS results, S was doped in the forms of S^{+4} and S^{+6} cations and oxidation state of Fe in TiO_2 lattice is Fe^{+3}. Based on the PL spectroscopy results, because of the defect formation in the doped TiO_2 thin film, this sample has lower PL intensity and consequently lower electron–hole recombination rate than TiO_2 thin film. Furthermore, co-presence of the S and Fe dopants in the structure of TiO_2 results in the remarkable narrowing of the band gap energy of TiO_2.

CONFLICTS OF INTEREST

The authors declare that there are no conflicts of interest regarding the publication of this manuscript.

REFERENCES

1. Chen X, Mao SS. Titanium Dioxide Nanomaterials: Synthesis, Properties, Modifications, and Applications. Chemical Reviews. 2007;107(7):2891-959.
2. Devi LG, Kavitha R. A review on non metal ion doped titania for the photocatalytic degradation of organic pollutants under UV/solar light: Role of photogenerated charge carrier dynamics in enhancing the activity. Applied Catalysis B: Environmental. 2013;140-141:559-87.
3. Kapilashrami M, Zhang Y, Liu Y-S, Hagfeldt A, Guo J. Probing the Optical Property and Electronic Structure of TiO2 Nanomaterials for Renewable Energy Applications. Chemical Reviews. 2014;114(19):9662-707.
4. Atay F, Akyuz I, Cergel MS, Erdogan B. Production and Characterization of (004) Oriented Single Anatase TiO2 Films. Journal of Electronic Materials. 2017;47(2):1601-10.
5. Humayun M, Raziq F, Khan A, Luo W. Modification strategies of TiO2 for potential applications in photocatalysis: a critical review. Green Chemistry Letters and Reviews. 2018;11(2):86-102.
6. Ohtani B. Titania Photocatalysis beyond Recombination: A Critical Review. Catalysts. 2013;3(4):942-53.
7. Periyat P, Pillai SC, McCormack DE, Colreavy J, Hinder SJ. Improved High-Temperature Stability and Sun-Light-Driven Photocatalytic Activity of Sulfur-Doped Anatase TiO2. The Journal of Physical Chemistry C. 2008;112(20):7644-52.
8. Li Y, Lv K, Ho W, Dong F, Wu X, Xia Y. Hybridization of rutile TiO 2 (rTiO 2) with g-C 3 N 4 quantum dots (CN QDs): An efficient visible-light-driven Z-scheme hybridized photocatalyst. Applied Catalysis B: Environmental. 2017;202:611-9.
9. Chinnusamy S, Kaur R, Bokare A, Erogbogbo F. Incorporation of graphene quantum dots to enhance photocatalytic

properties of anatase TiO2. MRS Communications. 2018;8(01):137-44.
10. Wang Z, Lang X. Visible light photocatalysis of dye-sensitized TiO2: The selective aerobic oxidation of amines to imines. Applied Catalysis B: Environmental. 2018;224:404-9.
11. Roose B, Pathak S, Steiner U. Doping of TiO2 for sensitized solar cells. Chemical Society Reviews. 2015;44(22):8326-49.
12. Keihan AH, Rasoulnezhad H, Mohammadgholi A, Sajjadi S, Hosseinzadeh R, Farhadian M, et al. Pd nanoparticle loaded TiO2 semiconductor for photocatalytic degradation of Paraoxon pesticide under visible-light irradiation. Journal of Materials Science: Materials in Electronics. 2017;28(22):16718-27.
13. Keihan AH, Hosseinzadeh R, Farhadian M, Kooshki H, Hosseinzadeh G. Solvothermal preparation of Ag nanoparticle and graphene co-loaded TiO2 for the photocatalytic degradation of paraoxon pesticide under visible light irradiation. RSC Advances. 2016;6(87):83673-87.
14. Zhang J, Xu LJ, Zhu ZQ, Liu QJ. Synthesis and properties of (Yb, N)-TiO2 photocatalyst for degradation of methylene blue (MB) under visible light irradiation. Materials Research Bulletin. 2015;70:358-64.
15. Taherinia M, Nasiri M, Abedini E, Pouretedal HR. Comparing the photocatalytic activity of N-doped and S-doped titanium dioxide nanoparticles for water splitting under sunlight radiation. Journal of the Iranian Chemical Society. 2018;15(6):1301-10.
16. Umebayashi T, Yamaki T, Yamamoto S, Miyashita A, Tanaka S, Sumita T, et al. Sulfur-doping of rutile-titanium dioxide by ion implantation: Photocurrent spectroscopy and first-principles band calculation studies. Journal of Applied Physics. 2003;93(9):5156-60.
17. Ohno T. Preparation of visible light active S-doped TiO2 photocatalysts and their photocatalytic activities. Water Science and Technology. 2004;49(4):159-63.
18. Ramacharyulu PVRK, Praveen Kumar J, Prasad GK, Sreedhar B. Sulphur doped nano TiO 2 : Synthesis, characterization and photocatalytic degradation of a toxic chemical in presence of sunlight. Materials Chemistry and Physics. 2014;148(3):692-8.
19. Shang X, Zhang M, Wang X, Yang Y. Sulphur, nitrogen-doped TiO2/graphene oxide composites as a high performance photocatalyst. Journal of Experimental Nanoscience. 2012;9(7):749-61.
20. Yang X, Cao C, Erickson L, Hohn K, Maghirang R, Klabunde K. Photo-catalytic degradation of Rhodamine B on C-, S-, N-, and Fe-doped TiO2 under visible-light irradiation. Applied Catalysis B: Environmental. 2009;91(3-4):657-62.
21. Mohamed SH, El-Hagary M, Althoyaib S. Growth of undoped and Fe doped TiO2 nanostructures and their optical and photocatalytic properties. Applied Physics A. 2012;111(4):1207-12.
22. Garg A, Singh A, Sangal VK, Bajpai PK, Garg N. Synthesis, characterization and anticancer activities of metal ions Fe and Cu doped and co-doped TiO2. New Journal of Chemistry. 2017;41(18):9931-7.
23. Tsay C-Y, Liang S-C. Ultraviolet-assisted annealing for low-temperature solution-processed p-type gallium tin oxide (GTO) transparent semiconductor thin films. Materials Science in Semiconductor Processing. 2017;71:441-6.
24. Pat S, Yudar HH, Korkmaz Ş, Özen S, Mohammadigharehbagh R, Pat Z. Transparent nano layered Li3PO4 coatings on bare and ITO coated glass by thermionic vacuum arc method. Journal of Materials Science: Materials in Electronics. 2017;28(24):19010-6.
25. Choi T, Kim J-S, Kim JH. Transparent nitrogen doped TiO2/WO3 composite films for self-cleaning glass applications with improved photodegradation activity. Advanced Powder Technology. 2016;27(2):347-53.
26. Lin Y-H, Tseng T-K, Chu H. Photo-catalytic degradation of dimethyl disulfide on S and metal-ions co-doped TiO2 under visible-light irradiation. Applied Catalysis A: General. 2014;469:221-8.
27. Gharagozlou M, Bayati R. Photocatalytic characteristics of single phase Fe-doped anatase TiO2 nanoparticles sensitized with vitamin B12. Materials Research Bulletin. 2015;61:340-7.
28. Tian F, Zhang Y, Zhang J, Pan C. Raman Spectroscopy: A New Approach to Measure the Percentage of Anatase TiO2 Exposed (001) Facets. The Journal of Physical Chemistry C. 2012;116(13):7515-9.
29. Brindha A, Sivakumar T. Visible active N, S co-doped TiO 2 / graphene photocatalysts for the degradation of hazardous dyes. Journal of Photochemistry and Photobiology A: Chemistry. 2017;340:146-56.
30. Nair PB, V.B.Justinvictor, Daniel GP, Joy K, Ramakrishnan V, Kumar DD, et al. Structural, optical, photoluminescence and photocatalytic investigations on Fe doped Tio2 thin films. Thin Solid Films. 2014;550:121-7.
31. Li H, Zhang X, Huo Y, Zhu J. Supercritical Preparation of a Highly Active S-Doped TiO2Photocatalyst for Methylene Blue Mineralization. Environmental Science & Technology. 2007;41(12):4410-4.
32. Gao H, Tian J, Zheng H, Tan F, Zhang W. Effects of Fe doping on the optical and magnetic properties of TiO2 films deposited on Si substrates by a sol–gel route. Journal of Sol-Gel Science and Technology. 2015;74(2):521-7.
33. Liqiang J, Yichun Q, Baiqi W, Shudan L, Baojiang J, Libin Y, et al. Review of photoluminescence performance of nano-sized semiconductor materials and its relationships with photocatalytic activity. Solar Energy Materials and Solar Cells. 2006;90(12):1773-87.
34. Gritsenko VA, Islamov DR, Perevalov TV, Aliev VS, Yelisseyev AP, Lomonova EE, et al. Oxygen Vacancy in Hafnia as a Blue Luminescence Center and a Trap of Charge Carriers. The Journal of Physical Chemistry C. 2016;120(36):19980-6.
35. Kim T, Hur J, Jeon S. The influence of interfacial defects on fast charge trapping in nanocrystalline oxide-semiconductor thin film transistors. Semiconductor Science and Technology. 2016;31(5):055014.
36. Tauc J. Absorption edge and internal electric fields in amorphous semiconductors. Materials Research Bulletin. 1970;5(8):721-9.
37. Wu G, Nishikawa T, Ohtani B, Chen A. Synthesis and Characterization of Carbon-Doped TiO2Nanostructures with Enhanced Visible Light Response. Chemistry of Materials. 2007;19(18):4530-7.
38. Wang MC, Lin HJ, Yang TS. Characteristics and optical properties of iron ion (Fe3+)-doped titanium oxide thin films prepared by a sol–gel spin coating. Journal of Alloys and Compounds. 2009;473(1-2):394-400.
39. Jiang H, Gao L. Enhancing the UV inducing hydrophilicity of TiO2 thin film by doping Fe ions. Materials Chemistry and Physics. 2003;77(3):878-81.
40. Liu R, Zhou X, Yang F, Yu Y. Combination study of DFT calculation and experiment for photocatalytic properties of S-doped anatase TiO2. Applied Surface Science. 2014;319:50-9.
41. Yang K, Dai Y, Huang B. Understanding Photocatalytic Activity of S- and P-Doped TiO2under Visible Light from First-Principles. The Journal of Physical Chemistry C. 2007;111(51):18985-94.